

Stress-Induced Gene Expression Sensing Intracellular Heating Triggered by Magnetic Hyperthermia

M. Elisa de Sousa, Alejandra Carrea, Pedro Mendoza Zélis, Diego Muraca, Olga Mykhaylyk, Yolanda E Sosa, Rodolfo G Goya, Francisco H. Sanchez, Ricardo A Dewey, and Marcela B. Fernández van Raap

J. Phys. Chem. C, **Just Accepted Manuscript** • DOI: 10.1021/acs.jpcc.5b12330 • Publication Date (Web): 10 Mar 2016

Downloaded from <http://pubs.acs.org> on March 10, 2016

Just Accepted

“Just Accepted” manuscripts have been peer-reviewed and accepted for publication. They are posted online prior to technical editing, formatting for publication and author proofing. The American Chemical Society provides “Just Accepted” as a free service to the research community to expedite the dissemination of scientific material as soon as possible after acceptance. “Just Accepted” manuscripts appear in full in PDF format accompanied by an HTML abstract. “Just Accepted” manuscripts have been fully peer reviewed, but should not be considered the official version of record. They are accessible to all readers and citable by the Digital Object Identifier (DOI®). “Just Accepted” is an optional service offered to authors. Therefore, the “Just Accepted” Web site may not include all articles that will be published in the journal. After a manuscript is technically edited and formatted, it will be removed from the “Just Accepted” Web site and published as an ASAP article. Note that technical editing may introduce minor changes to the manuscript text and/or graphics which could affect content, and all legal disclaimers and ethical guidelines that apply to the journal pertain. ACS cannot be held responsible for errors or consequences arising from the use of information contained in these “Just Accepted” manuscripts.



1
2
3
4
5
6
7
8
9
10
11
12
13
14
15
16
17
18
19
20
21
22
23
24
25
26
27
28
29
30
31
32
33
34
35
36
37
38
39
40
41
42
43
44
45
46
47
48
49
50
51
52
53
54
55
56
57
58
59
60

Stress-induced Gene Expression Sensing Intracellular Heating Triggered by Magnetic Hyperthermia

M. Elisa de Sousa ^{a†}, Alejandra Carrea ^{b††}, Pedro Mendoza Zélis ^a, Diego Muraca ^c, Olga Mykhaylyk ^d, Yolanda E. Sosa ^e, Rodolfo G. Goya ^e, Francisco H. Sánchez ^a, Ricardo A. Dewey ^b,
Marcela B. Fernández van Raap ^{a,*}

^a Instituto de Física La Plata (IFLP- CONICET), Departamento de Física, Facultad de Ciencias Exactas, Universidad Nacional de La Plata (UNLP), Argentina

^bInstituto de Investigaciones Biotecnológicas-Instituto Tecnológico de Chascomús, (IIB-INTECH), CONICET/UNSAM, Chascomús, Argentina

^cInstituto de Física “Gleb Wataghin” (IFGW), Universidade Estadual de Campinas, Brazil

^dInstitut für Experimentelle Onkologie und Therapie Forschung Technische Universität München, Germany

^e Instituto de Investigaciones Bioquímicas de La Plata INIBIOLP, Facultad de Medicina, UNLP, Argentina

* Corresponding Author: M. B. Fernández van Raap
E. mail address: raap@fisica.unlp.edu.ar
Mail address: c.c 67, (1900) La Plata, Argentina.
Phone: +54 221 4246062 x 257, Fax +54 221 4236335

Present Addresses

† INIFTA, Instituto de Investigaciones Fisicoquímicas de La Plata. Argentina

†† Centro Regional de Estudios Genómicos, Facultad de Ciencias Exactas, Universidad Nacional de La Plata, Argentina

ABSTRACT

It is known that alternating magnetic field applications on eukaryotic cells loaded with single domain iron oxide nanoparticles result in high hyperthermic cytotoxicity leading to cell death. Although magnetic hyperthermia therapy for cancer tumours is being developed under this idea, some *in vitro* assays have shown controversial results indicating that alternating magnetic field triggers large apoptotic effect without significant culture-temperature increase. In agreement with these observations a huge lowering in nanoparticle specific heating rates, when going from the colloidal suspension to cell endosomes, together with cell death, has been reported. Here, we propose a new methodology to determine the occurrence of local heating in cells when alternating magnetic fields in the radiofrequency field range are applied to cell cultures holding very low iron oxide concentrations, being these concentrations insufficient to produce a global cell-culture temperature increase up to therapeutic values. To this end, human lung adenocarcinoma cells (A549 cell line) were transduced with a lentiviral vector encoding the expression of the enhanced green fluorescence protein, EGFP, under the action of the inducible human heat shock protein 70B promoter. This modified A549 cell line was incubated with aqueous suspensions of magnetite core nanoparticles (uncoated or covered with coating agents like citric acid or silicon oxide), and exposed to radiofrequency fields. The application of an alternating magnetic field to cell cultures loaded with nanoparticles resulted in no global temperature increase but EGFP expression. Stress-inducible gene expression scales with uptake

1
2
3 and nanoparticle properties like saturation magnetization and heat dissipation efficiency. Our
4
5 analysis demonstrates that EGFP expression is linked to a localized intracellular temperature
6
7 increase.
8
9

10
11 KEYWORDS magnetic hyperthermia, intracellular heating, iron-oxide nanoparticles, human
12
13 HSP70B promoter, enhanced green fluorescence protein, radio frequency magnetic field.
14
15
16
17
18
19

20 **Introduction**

21
22
23 Nowadays cancer is one of the main causes of death, with millions of individuals being newly
24
25 diagnosed every year. The risk of getting cancer before the age of 75 is 18.5 %, while the risk of
26
27 dying from cancer is 10 %¹. This situation is leading to the development of new diagnosis and
28
29 therapeutics protocols involving the use of nanoactuators, nanobiodevices and nanoscience
30
31 methodologies. Oncologic nanotherapies include Magnetic Hyperthermia (MH)², Plasmonic
32
33 Photothermal Therapy³, targeted delivery of anticancer drugs and genes⁴, and Photodynamic
34
35 Therapy⁵. These new therapies are meant to be less invasive, more efficient and displaying minor
36
37 side effects.
38
39
40
41
42

43
44 The MH oncologic therapy is based on the ability of magnetic nanoparticles (MNPs) to induce
45
46 cancer-cell death upon exposure to an alternating magnetic field (AMF). This AMF is typically of
47
48 a field driven frequency around 100 kHz and a field amplitude of 15 kA/m. It is believed that
49
50 cancer cells are killed only when the tumour temperature is raised above 42 °C. Cancer-cell
51
52 death is due to pathobiological effects such as modification of the normal structures of
53
54 phospholipids, proteins, and nucleic acids, leading to the deterioration of cell-structure integrity⁶.
55
56
57
58
59
60

1
2
3 MH therapy is already under clinical trials⁷. Although a great breakthrough has been achieved in
4 many aspects involved in the establishment of this methodology (by itself or combined with
5 more conventional methodologies like radio and chemo therapies), a series of controversial *in*
6 *vitro* results have been reported. In these experiments, cell death was achieved without an
7 average global temperature increase of the cell culture⁸⁻¹⁰. For instance, Villanueva et al.⁸ have
8 shown that the application of an AMF (100 kHz and 12 kA/m) to HeLa tumour cells previously
9 incubated with silica-coated manganese oxide, induced significant cellular damage leading to
10 cell death, although the temperature increase in the cell culture (initially at 37 °C) during the MH
11 treatment was lower than 0.5 °C. Marcos-Campos et al.⁹ have reported a viability decrease from
12 90 % to 2-5 % in monocyte-derived dendritic cells, previously loaded with positively and
13 negatively charged magnetite nanoparticles (coated with COOH- or with NH₂⁺ functional
14 groups), after 30 min exposure to an AMF of 260 kHz and 13 kA/m. In spite of this, only a
15 temperature increase of 2 °C, over an initial value of 26 °C, was registered. More recently,
16 DiCorato et al.¹⁰ have carried out systematic measurements of both hyperthermia and magnetic
17 properties in controlled cell environments, using human ovary adenocarcinoma SKOV-3 cells
18 and a wide range of nanomaterials. These authors have reported a systematic fall in the heating
19 efficiency for nanomaterials associated with tumour cells. In agreement with these experiments
20 dealing cells that have internalized the MNPs by unspecific way, similar results have been also
21 shown for *in vitro* experiments involving more complex receptor-mediated endocytosis process.
22 Creixell et al.¹¹ have analysed the internalization of iron oxide nanoparticles coated with
23 carboxymethyl dextran and conjugated to epidermal growth factor (EGF) in breast human MDA-
24 MB-468 and MCF-7 cells. The binding of EGF to the epidermal growth factor receptor resulted
25 in a significant reduction in cell viability and in a clonogenic survival up to 40 % in a thermal-
26
27
28
29
30
31
32
33
34
35
36
37
38
39
40
41
42
43
44
45
46
47
48
49
50
51
52
53
54
55
56
57
58
59
60

1
2
3 heat dose-dependent manner. It was found that viability reduction further increased up to 99.9 %
4
5 by 120 min application of AMF of 233 kHz and 37.5 kA/m, but without a perceptible
6
7 temperature rise during the experiment. Domenche et al.¹² have reported the manipulation of
8
9 lysosome-membrane permeability for selectively killing cancer cells by targeting MNPs to the
10
11 lysosome and exposing them to an AMF of 233 kHz and 42 kA/m. These authors have suggested
12
13 that energy dissipated by MNPs associated to lipid membranes under an AMF, leads to the
14
15 membrane permeabilization. They have also shown that this effect correlates with the production
16
17 of reactive oxygen species and with a decrease in tumour cell viability. Amstad et al.¹³ have
18
19 shown that upon AMF application, iron-oxide containing liposomes delivered their cargo, even
20
21 though the heat released was insufficient to reach membrane melting temperature.
22
23
24
25
26

27
28 These results cast doubt on the causes and mechanisms involved in cell death during MH
29
30 treatments. MNPs dispersed in fluid, gel or solid matrix are known to release heat through Néel
31
32 and/or Brown relaxation mechanisms when they are exposed to AMFs¹⁴. The heat dissipation is
33
34 related to the out of phase magnetic susceptibility due to the phase lag of the magnetic response
35
36 behind the applied field. However, cell-internalized MNPs group inside endosomes of about 1-2
37
38 μm size, constituting magnetic endosomes which themselves have a resultant magnetic moment.
39
40 These magnetic endosomes can align in the direction of an applied field forming chains¹⁵. In this
41
42 case, the MNPs may locally release heat due to the relaxation of the MNP magnetic moment
43
44 and/or due to the elastic and viscous response of the cell cytoskeleton to the mechanical rotation
45
46 and vibration of the magnetic endosome. Microrheology and measurements of the intrinsic strain
47
48 fluctuations of living cells have shown that the cytoskeleton is a highly dynamic, actively
49
50 stressed network that can be treated as a coarse-grained continuum¹⁶. On the other hand, the
51
52
53
54
55
56
57
58
59
60

1
2
3 motion of aligned magnetic endosomes of microbeads engulfed by *Dictyostelium* cells has been
4 reported¹⁵.
5
6

7
8 Although various *in vitro* experiments have shown cell death without global culture temperature
9 increase, attempts to experimentally determine intracellular temperature increase are rare. Most
10 common techniques for monitoring intracellular temperature use thermosensitive dyes whose
11 fluorescence properties depends on temperature. A temperature probe, based on the thermal
12 decomposition of a thermo-sensitive azobis[N-(2-carboxyethyl)-2-methylpropionamidine]
13 molecule, has been employed to probe the temperature profile at the surface of iron oxide
14 nanoparticle functionalized with poly(ethylene glycol) when they are exposed to AMF. In that
15 setup the fluoresceineamine dye was attached to a thermo labile azo linker and dye release was
16 monitored by photoluminescence¹⁷. Alternatively, temperature probing has been achieved by
17 monitoring the fluorescence polarization anisotropy of GFP. The method was tested on GFP
18 transfected HeLa and U-87 MG cancer cell lines surrounded by gold nanorods exposed to
19 photothermal heating¹⁸.
20
21
22
23
24
25
26
27
28
29
30
31
32
33
34
35
36

37 Here, we attempt to fill this point by means of measuring the stress-inducible gene expression in
38 modified A549 cells that express EGFP when internalized with MNPs and exposed to an AMF.
39 The lentiviral vector used to modify A549 cells contains the stress-inducible internal human
40 HSP70B promoter, which directs EGFP expression. These modified A549 cells (from now on
41 A549^{HSP}) were incubated with different Fe₃O₄ MNPs: uncoated (u), citric acid coated (CA), and
42 silicon oxide coated (SiO_x); and were exposed to an AMF of 128 kHz and 20.3 kA/m. Flow
43 cytometry analysis was used to monitor temperature-inducible EGFP expression at single-cell
44 level without any additional processing steps. We showed that stress-inducible gene expression
45 in a modified A549 cell line, which has EGFP sequence under the action of HSP70B promoter
46
47
48
49
50
51
52
53
54
55
56
57
58
59
60

1
2
3 (inducible with temperature), is linked to the intracellular MNPs heat dissipation. This link
4
5 strongly suggests that endocytosed MNPs create hot spots inside the cells, even though the amount
6
7 of heat released is not enough to globally increase the cell culture temperature.
8
9

10 11 **Materials and methods**

12 13 **Aqueous magnetic suspension synthesis and characterization**

14
15
16
17
18 Stable aqueous dispersions of uncoated and citric acid coated magnetite were prepared from iron
19
20 chlorides as previously described¹⁹. Briefly, 2.75 g of $\text{FeCl}_3 \cdot 4\text{H}_2\text{O}$ and 1.01 g of $\text{FeCl}_2 \cdot 6\text{H}_2\text{O}$
21
22 were dissolved in 50 ml of bidistilled water each, mixed in a three-neck flask, and heated to the
23
24 reaction temperature of 60 °C. Then, 3 ml of ammonia solution (AS) NH_4OH (25 % w/w) was
25
26 added drop by drop and left to react for 30 min. After that, 75 ml of AS were added at a rate of
27
28 1 drop/s until the solution reached a pH of 10.5, high enough to prevent agglomeration due to
29
30 surface charge. Then, the black precipitate was separated from the dispersion medium with a
31
32 permanent magnet and resuspended in water at physiological pH ~ 7.4 to get uncoated magnetite
33
34 (Fe_3O_4), or mixed with citric acid (CA) aqueous solution (0.02 g/ml) at pH 4 and left to react for
35
36 90 min at 60 °C to get citric acid coated magnetite (CA- Fe_3O_4). Finally, the MNPs were
37
38 resuspended in water at physiological pH, around 7.4. The surface carboxylate groups provide
39
40 electrostatic stabilization. Chemical volumetric analysis was used to determine the concentration
41
42 [x] of these colloid with an accuracy of 2%. [x] is expressed as magnetite mass per solvent
43
44 volume. $\text{K}_2\text{Cr}_2\text{O}_7$ was used as titrant.
45
46
47
48
49
50

51
52
53 Silica-iron oxide ($\text{SiO}_x\text{-Fe}_3\text{O}_4$) MNPs were synthesized by means of precipitation of
54
55 Fe(II)/Fe(III) hydroxide from the aqueous solution of the mixture of Fe(II) and Fe(III) salts,
56
57

1
2
3 followed by transformation into magnetite in an oxygen-free atmosphere. The surface coating
4 resulted from the hydrolysis and condensation of tetraethyl orthosilicate (TEOS) and 3-
5 (trihydroxysilyl) propylmethylphosphonate (THPMP) and 3-mercaptopropyltrimethoxysilane,
6 yielding a silicon oxide layer with surface phosphonate groups (SiO_x/Phosphonate)^{20, 21}. Briefly,
7
8 6.8 g of ferric chloride hexahydrate and 2.5 g of ferrous chloride tetrahydrate in 200 ml ddH₂O
9
10 water were treated with 15 ml concentrated ammonium hydroxide to obtain a primary
11
12 precipitate. The material was heated to 90 °C for 15 min and then stirred at this temperature for
13
14 30 min. To form a coating, 375 μl (1.9 mmol) of TEOS was added. After 30 min, 750 μl of 42 %
15
16 THPMP solution (1.3 mmol) and 150 μl (0.72 mmol) of 3-mercaptopropyltrimethoxysilane were
17
18 added. The mixture was further treated at 90°C for another 30 min, cooled to 25°C, diluted twice
19
20 with ethanol, and incubated for 24 h with continuous stirring. The particles were separated using
21
22 a magnet and washed twice with ethanol and once with water. The product was sonicated for 10
23
24 min. In this way, magnetite nanoparticles coated silicon oxide layer with surface phosphonate
25
26 groups (SiO_x-Fe₃O₄) well dispersed in aqueous solution were obtained. The surface phosphonate
27
28 groups provide electrostatic stabilization. Colloid concentration was determined
29
30 spectrophotometrically by forming complexes with 1,10-phenanthroline²⁰.
31
32
33
34
35
36
37
38
39
40
41

42 Transmission electron microscopy (TEM) images were measured with a JEOL JEM 2100TEM
43 (acceleration voltage 200 kV, Spot Size 1, Alpha Selector 3) and JEOL JEM 3010 HR-TEM
44 (acceleration voltage 300 kV, Spot Size 1, Alpha Selector 3). Samples were prepared by drying
45
46 the dispersed nanoparticles on a carbon-coated copper grid (ultrathin carbon/holey carbon, 400
47
48 mesh cooper grid). The images were acquired with the sample on a single-tilt sample holder
49
50 using Gatan MSC798 TV camera, Gatan Digital Micrograph and EMMENU programs.
51
52
53
54
55
56
57
58
59
60

Alternating magnetic field application

For AMF application, a field generator consistent of a 2.5 kV power supply and a resonant RLC circuit Hüttinger (2.5/300) was used. The resonator holds an external exchangeable water refrigerated coil. The sample is placed in its centre. For determining the SAR of MNPs in aqueous suspensions a 6-turn coil of 2.5 cm diameter was used, while for living-cell experiments a 5-turn coil of 7 cm diameter was used because it was more suitable for placing in its interior a thermal bath at 37 °C with a Petri dish inside.

To calorimetrically evaluate the SAR of the MNP colloids, a sample of 0.5-1.0 mL was poured in a clear glass Dewar, and exposed to 128, 170 and 260 kHz and field amplitude varying in the range from 16 to 52 kA/m. An optical fiber sensor connected to a calibrated signal conditioner (Neoptix) with an accuracy of ± 0.1 °C was used to measure the colloid temperature during the experiment. The sensor was placed in the center of the sample. Field application was interrupted before reaching 50 °C, in order to minimize solvent evaporation and prevent its destabilization.

The SAR values were calculated from the initial slope $\partial T / \partial t$ of experimental heating curves as

$$SAR = \frac{C_V}{[x]} \frac{\partial T}{\partial t}$$
 where C_V is the volumetric heat capacity of the solvent (4.18 J/cm³ K) and [x] the

colloid concentration as determined by chemical analysis. [x] is expressed as magnetite mass per solvent volume. This value was used to normalize magnetization data and to determine experimental SAR values. Each SAR value was determined from three independent experimental heating curves.

Cell culture conditions

1
2
3 Human lung adenocarcinoma cell line A549 (ATCC, CCL-185) was cultured in Dulbecco's
4 modified Eagle's medium (Gibco, Life Technologies, Denmark) supplemented with 10 % fetal
5 bovine serum, FBS, (NATOCOR, Cordoba, Argentina), 1% penicillin/streptomycin (Gibco Life
6 Technologies, USA), and 1% glutamine solution (Gibco Life Technologies, USA), at 37 °C in a
7 humidified 5 % CO₂ incubator, unless specified otherwise.
8
9
10
11
12
13
14
15

16 **Lentiviral vector generation**

17
18
19 Cell-free lentiviral supernatants were generated by transient cotransfection of 293T packaging
20 cell line with one of the two transfer vector used in this study (CMV/EGFP or HSP/EGFP,
21 kindly provided by F. Noyan et al.²²), together with the packaging constructs: the Gag/Pol-
22 expressing plasmid (pMDLg/pRRE), the Rev-expressing plasmid (pRSV-REV) and the envelope
23 plasmid (pCMV-VSVG), as previously described²³. Viral titers were determined on A549 cells
24 in the presence of 1mg ml⁻¹geneticin for 2 weeks, yielding vector titers of 10⁶-10⁸ TU
25 (transducing units) ml⁻¹.
26
27
28
29
30
31
32
33
34
35
36

37 **Transduction of A549 cell line**

38
39
40 A549 cells were transduced with either CMV/EGFP or HSP/EGFP lentiviral vectors at a
41 multiplicity of infection of 50, for 72 h in the presence of 8 µg ml⁻¹polybrene (Sigma-Aldrich, St.
42 Louis, USA). After incubation in medium containing 1 mg ml⁻¹geneticin for 2 weeks, individual
43 neomycin-resistant clones were isolated and subcultured, generating the cell lines A549^{CMV}
44 (constitutive EGFP expression) and A549^{HSP} (inducible EGFP expression). Control-induction of
45 EGFP expression in A459^{HSP} cell line was achieved by incubating the cells at 43 °C for 60 min,
46 followed by incubation at 37 °C for 24 h. EGFP expression was detected by flow cytometry
47 using a FACSCalibur flow cytometer (BD Biosciences).
48
49
50
51
52
53
54
55
56
57
58
59
60

10

Cell culture conditions for AMF application

For AMF application, $\sim 10^5$ A549 or A549^{HSP} cells were grown in Petri dish (diameter 2.3 cm) with 2 ml of medium containing 0.5 mg ml^{-1} geneticin. When 60 % confluence was reached, cells were washed with phosphate buffered saline (PBS) and incubated for another 17 h in medium doped with the MNPs at a concentration of $29 \text{ } \mu\text{g}_{\text{Fe}_2\text{O}_4}/\text{ml}$. Cells were then washed four times with PBS to remove the non-incorporated MNPs, and medium was replaced. This procedure was carried out with three types of MNPs $\alpha\text{-Fe}_3\text{O}_4$, $\text{AC-Fe}_3\text{O}_4$ or $\text{SiO}_x\text{-Fe}_3\text{O}_4$. Immediately, the Petri dishes containing the cells internalized with MNPs with the monolayer covered with 1 mm layer of DMEM, were placed in a double-wall vessel filled with circulating water at controlled temperature of $37 \text{ }^\circ\text{C}$, and exposed for 135 min to an AMF of 128 kHz and 20.3 kA/m. After exposure to the AMF, medium was replaced and the cell cultures were incubated under controlled conditions for 24 h. For cytometry measurements, the cultures were harvested from each dish by trypsination, and fixed with paraformaldehyde (4 %) for 20-25 min, resuspended in PBS, and then stored at $4 \text{ }^\circ\text{C}$ until measurements. Cells grown at the same conditions as those of the internalized ones, but without MPNs, were used as control.

Internalization, localization and uptake quantification

TEM was used to visualize MNPs localization inside the cells. After incubation with magnetic colloids labelling, adhered cells were washed two times with PBS, and then incubated in 2% glutaraldehyde in phosphate buffer and distilled water for 2 h at $4 \text{ }^\circ\text{C}$. Cells were then postfixed in 1% OsO_4 for 2 h at $4 \text{ }^\circ\text{C}$, washed again with phosphate buffer, dehydrated in an alcohol series, and embedded in Epoxy resin. Ultrathin sections of 60 nm, cut with Reichert-J Super Nova

1
2
3 ultramicrotome, were examined with a JEOL 1200 EX II transmission electron microscope.

4
5 Images were acquired with Gatan Erlangshen ES 1000W digital camera.

6
7
8
9 DC magnetometry was used to determine MNP cell-uptake. Specific magnetization (M) as a
10
11 function of applied magnetic field (H) at room temperature was obtained using vibrating sample
12
13 magnetometer (VSM) LakeShore 7404, operated with maximum applied fields $\mu_0 H_{max}=1.5$ T.

14
15
16 For sample preparation, the same growth and incubation protocols as described above were
17
18 followed but, in order to reach VSM sensitivity, cells were grown in 75 cm² flasks with 16 ml of
19
20 medium. After growth and incubation with MNPs, cells were washed, harvested by
21
22 trypsinization, resuspended in 15 ml of PBS and counted in a Neubauer chamber. From
23
24 magnetization vs. applied field curves of cells incubated with MNPs and of the same MNPs in
25
26 aqueous suspensions, the mean uptake C , expressed in pg Fe₃O₄/cell, was obtained as

27
28
29
30
31 $10^{15} m_s (Am^2) / M_s (Am^2 / kg_{Fe_3O_4}) N_{cell}$, where m_s is the magnetic moment at saturation of the cells
32
33 incubated with MNPs, M_s is the specific saturation magnetization of the MNPs and N_{cell} is the
34
35 number of cells in the sample. VSM measurements were carried out on liquid colloid at room
36
37 temperature to determine M_s . To this end, 50 μ L of colloidal suspension were sealed into a
38
39 heat shrinkable tube to prevent sample evaporation and spills. The so determined colloid
40
41 magnetic moment was divided by the mass of Fe₃O₄ contained in the sealed volume of
42
43 colloidal suspension.
44
45
46
47

48 49 **Statistical analyses**

50
51
52
53 Comparisons between two samples were performed using Student's t test. p -values < 0.05 were
54
55 considered statistically significant.
56
57

Results and discussion

The ability of an assembly of MNPs to induce hyperthermia upon exposure to an AMF (driven field frequency f and field amplitude H_0) depends markedly on their physical properties and on the environment where they are located. In general, the specific absorption rate SAR is a parameter that characterizes the ability of an assembly of MNPs (single magnetic domain), of volume V and density ρ , dispersed in a medium of viscosity η , to release heat under an AMF.

This parameter is given by: $SAR = \mu_0 \pi f H_0^2 V \chi''(f, \tau)$, where μ_0 is the free space permeability

($4\pi \cdot 10^{-7}$ H/m) and $\chi''(f, \tau) = \frac{2\pi f \tau}{1 + (2\pi f \tau)^2} \chi_0$ is the out-of-phase magnetic susceptibility with

$\chi_0 \cong \frac{\mu_0 \rho M_s^2 V}{3k_B T}$. Then, besides preset AMF parameters (f and H_0), heating is governed by the

MNPs effective relaxation time τ given by: $\tau^{-1} = \tau_N^{-1} + \tau_B^{-1}$, where Néel relaxation is due to the

switching of the particle magnetic-moment within a time $\tau_N = \tau_0 \exp(K_e V / k_B T)$ and Brown

relaxation is due to the particle rotation within a time $\tau_B = \frac{3\eta V_H}{k_B T}$. Clearly, MNPs susceptibility

and SAR parameter depend in a complex way on the MNP properties like: size (D), size

dispersion, hydrodynamic volume (V_H), saturation magnetization (M_s), and effective anisotropy

constant (K_e). The uncoated, citric acid coated, and silicon oxide coated MNPs used in this work

were synthesized by the co-precipitation method, and their physical properties were determined

by TEM, VSM and magnetocalorimetric measurements.

1
2
3 Mean sizes $\langle D \rangle$ were derived from size histograms obtained through many TEM images of the
4 MNPs. Representative images and the fitted number log-normal distribution are shown in figure
5
6
7
8
9
10
11
12
13
14
15
16
17
18
19
20
21
22
23
24
25
26
27
28
29
30
31
32
33
34
35
36
37
38
39
40
41
42
43
44
45
46
47
48
49
50
51
52
53
54
55
56
57
58
59
60

Mean sizes $\langle D \rangle$ were derived from size histograms obtained through many TEM images of the MNPs. Representative images and the fitted number log-normal distribution are shown in figure 1 for the three MNPs. Other images and specific data analysis for each MNP are displayed in figures 1, 2, and 3 of Electronic Supplementary Material (ESM). For the three MNP types, crystal planes are observed and electron diffraction (ED) patterns were well indexed with the with a cubic spinel structure, space group $Fd3m$ of magnetite and maghemite phases, (see figure 1e). In the case of SiO_x -MNPs, the thickness of the silica shell, as estimated from the non crystalline flanges observed in TEM images as those shown in figure 3 of ESM, is around 1 nm.

Magnetic characterization shown in figure 2a indicates that the particles are single magnetic-domains, and small enough so that M vs. H loops display no hysteresis at room temperature. The loops were well fitted with Langevin functions and accurate M_s values were derived from these fits. The K_e value was assumed to be the same for the three MNPs used here. Heating curves measured during the application of 128 kHz and 20.3 kA/m field on the colloidal suspension of concentration $[x]$, listed in table 1, are shown in figure 2b. The M_s value of CA-MNP is almost half of the magnitude determined for u-MNP, although the MNP sizes of both particles are very close. This result is in agreement with previous work¹⁹ where we have shown that citric acid coating influence the surface of the iron oxide nanoparticles, producing a larger magnetic frustrated layer, improving nanoparticle stability in the suspension but lowering M_s and SAR values. SiO_x -MNP falls out of this behaviour, M_s is close to magnetite bulk i.e. no frustrated layer appears. The SAR of SiO_x -MNP is lower than the SAR of u-MNP. This is a quite interesting result having SiO_x -MNP larger size and larger M_s , that may be related to the insulating characteristic of silicon oxide covering layer.

1
2
3 These particles, displaying distinctive structuring, M_s , and fluid SAR values, were chosen to
4 experimentally determine the occurrence of intracellular temperature increase in A549 cell
5 culture. The relevant magnetic and structural properties are listed in table 1.
6
7

8
9
10
11 The magnetic susceptibility $\chi''(f, \tau)$ appearing in SAR formula, displays a maximum at the
12 condition $2\pi f\tau = 1$. In figure 3, SAR-frequency dependence is exemplified for $SiO_x-Fe_3O_4$. A
13 maximum value of 67.3 W/g was registered within the available frequency range, at 128 kHz,
14 while $CA-Fe_3O_4$ displays a monotonous increasing behaviour (see figure 2 of ESM), with
15 maximum SAR value measured at 15 W/g at 170 kHz. With the aim of evaluating intracellular
16 MH by means of assessing EGFP expression, the field parameters that maximize fluid SAR of
17 $SiO_x-Fe_3O_4$ were chosen for *in vitro* experiments with A549^{HSP} cells loaded with nanoparticles,
18 for each type of MNP.
19
20
21
22
23
24
25
26
27
28
29
30

31
32 Once MNPs were well characterized, we proceed to analyze their interactions with the cells. To
33 this end, the amount and location of internalized MNPs were evaluated. Figure 4 shows
34 representative TEM images showing the distribution of the CA-MNPs inside the cell. The
35 particles were incorporated by an unspecific endocytosis process and located inside cytoplasm
36 vesicles. Uptake amounts for the three types of MNPs were determined after 17 h of incubation
37 with medium doped to 29 $\mu\text{g}_{\text{MNP}}/\text{ml}$ of culture medium (DMEM) using dc-magnetometry, as
38 described in Materials and methods section. Different uptake values, listed in table 2, were
39 obtained for the different particles, probably because cell uptake capacity depends on MNP
40 coating. During this process, the particles first bind to the plasma membrane in the form of
41 clusters, later they are engulfed inside the cell. Binding and cluster formation depend on coating
42
43
44
45
46
47
48
49
50
51
52
53
54
55
56
57
58
59
60

1
2
3 type and charge²⁴. The qualitative uptake, as visualized from TEM images, is consistent with
4
5 uptake values measured with dc magnetometry.
6
7

8
9 Then, thermal induction of gene expression in A549^{HSP} cells was assessed by detecting EGFP
10 expression after treatments at 37, 39 and 43 °C for 60 min, using flow cytometry analysis. The
11 percentage of cells expressing EGFP (% EGFP) linearly increases with temperature to reach a
12 maximum of about 80 % at 43 °C, relative to EGFP expression of untreated cells. Results are
13 shown in figure 5, together with representative optical and fluorescence images and a
14
15 representative flow cytometry dot plot. This analysis confirms that thermal stress is able to
16
17 induce EGFP expression in A549^{HSP} cells, and this induction is greatly increased at 43 °C, as
18
19 previously reported²².
20
21
22
23
24
25
26
27

28
29 Figure 6 shows the results of experiments carried out to determine whether exposure to an AMF
30 or MNP incorporation into the cell endosomes could induce stress by themselves. The
31 percentages of cells expressing EGFP after exposure to an AMF (128 kHz and 20.3 kA/m)
32 during $t_a=15, 30, 60, 135, 150$ y 180 min are shown in figure 6a. For $t_a \leq 60$ min the increase in
33
34 %EGFP (relative to negative control) was lower than 2 %. For $t_a=180$ min the increase of EGFP
35
36 was about 25 %, while for times shorter than 135 min the increases were below 8 %. Regarding
37
38 MNP-uptake experiments, the percentages of cells expressing EGFP after incubation with 5, 18,
39
40 29, 58 y $116 \mu\text{g}_{\text{Fe}_3\text{O}_4}/\text{ml}_{\text{DMEM}}$ of $\text{SiO}_x\text{-Fe}_3\text{O}_4$ colloidal suspension are shown in figure 6b. When
41
42 incubating with $58 \mu\text{g}_{\text{Fe}_3\text{O}_4}/\text{ml}_{\text{DMEM}}$, an increase of EGFP, relative to negative control, of about 23
43
44 % was observed. Therefore, to avoid induction originated by exposure to an AMF itself or by
45
46 MNP uptake itself, we have chosen $29 \mu\text{g}_{\text{Fe}_3\text{O}_4}/\text{ml}_{\text{DMEM}}$ as a suitable concentration for incubation
47
48 and AMF exposing times shorter than 150 min.
49
50
51
52
53
54
55
56
57
58
59
60

1
2
3 Finally, to evaluate the occurrence of intracellular MH in A549^{HSP} cells loaded with Fe₃O₄, AC-
4 Fe₃O₄ or SiO_x-Fe₃O₄ MNPs, the following procedure was carried out. Cells were grown as
5
6 monolayer in 5 Petri dishes, and the percentage of EGFP was evaluated in: 1) cells treated for 60
7
8 min at 43 °C (positive control) to corroborate that the promoter was properly working; 2) cells
9
10 incubated without MNPs and not exposed to any AMF or thermal treatment (negative control), to
11
12 be aware of any random unpredictable source of stress; 3) cells incubated for 17 h in medium
13
14 doped with the MNPs at a concentration of 29 μg_{Fe₃O₄}/ml_{DMEM} and not exposed to any AMF or
15
16 thermal treatment (MNPs-control); 4) cells exposed to an AMF for 135 min without MNPs
17
18 incubation or any thermal treatment (AMF-control); and 5) cells incubated with MNPs at a
19
20 concentration of 29 μg_{Fe₃O₄}/ml_{DMEM} and exposed to an AMF of 128 kHz and 20.3 kA/m for 135
21
22 min (MH-experiment). This procedure was carried out with the three different MNPs: Fe₃O₄,
23
24 CA-Fe₃O₄ and SiO_x-Fe₃O₄, in duplicate.
25
26
27
28
29
30
31
32

33 Culture temperature was sensed during the whole exposure time to the AMF and no temperature
34
35 increase was registered in any experiment, consistently with previous results discussed in the
36
37 introduction. Then, intracellular SAR cannot be magneto-calorimetrically established.
38
39
40

41 Results of the percentage of EGFP expressing cells for these five cell cultures (controls and MH
42
43 experiment) for the three MNPs are shown in figure 7. The basal levels of EGFP expression in
44
45 the negative control cells were similar to the values seen in the AMF-control ($p=0.75231$), and to
46
47 the percentage of EGFP expression observed in cells treated with all three MNPs-controls: Fe₃O₄
48
49 ($p=0.99525$), AC-Fe₃O₄ ($p=0.48913$), and SiO_x-Fe₃O₄ ($p=0.59582$). These results indicated that
50
51 neither the field nor the particle uptake induced stress by themselves. Contrarily, cells incubated
52
53 with all of the three types of MNPs and exposed to the AMF (MH-experiment) shown
54
55
56
57
58
59
60

1
2
3 statistically significant differences in the percentage of EGFP expressing cells compared to the
4 cells treated with the same MNPs (p equal to 0.02253, 0.00275, and 0.06674 for u-Fe₃O₄, SiO_x-
5 Fe₃O₄, and AC-Fe₃O₄, respectively), and compared to the corresponding AMF controls (p equal
6 to 0.00286, 0.00162 and 0.0102 for Fe₃O₄, SiO_x-Fe₃O₄, and AC-Fe₃O₄, respectively). These
7 results gave evidence that the HSP70B promoter was able to increase EGFP gene expression
8 upon MNP-driven hyperthermia.
9

10
11
12 Subsequently, we analyzed gene expression induction in culture cells incubated with the three
13 types of MNPs and exposed to AMF, using the distinctive MNPs physical parameters and SAR
14 behaviour.
15

16
17
18 Although the amount of heat dissipated in the cell cultures was not enough to significantly raise
19 the cell culture temperature to allow the calorimetric measure of the intracellular SAR, we found
20 a correlation between SAR measured in the aqueous suspension and the percentage of loaded
21 A549^{HSP} cells expressing EGFP after exposure to the AMF. The larger the SAR value, the larger
22 the % EGFP (see figure 8a). Assuming that these SAR values holds in the cell environment, the
23 total heat dose (THD) expressed in joules per cell²⁵ was calculated using SAR values at a given
24 magnetic-field frequency and amplitude, the application time t_a , and the mass of internalized
25 nanoparticles per cell (C) as: $THD = C \times SAR \times t_a$. Using uptake values C determined with a dc
26 magnetometer, listed in table 2, THD values of 1.16, 4.08 and 15.32 $\mu\text{J}/\text{cell}$ were obtained for
27 AC-, SiO_x- and u- MNPs, respectively. Figure 8b shows that the percentage of loaded A549^{HSP}
28 cells expressing EGFP after exposure to the AMF increases with THD, i.e. the % EGFP
29 increases with the mean energy released per cell. It can be notice that the relation between the %
30 EGFP and THD is not linear. A linear relation could have been expected having in mind the
31
32
33
34
35
36
37
38
39
40
41
42
43
44
45
46
47
48
49
50
51
52
53
54
55
56
57
58
59
60

1
2
3 linear relation obtained for homogeneous heating of A549^{HSP} cells in thermal bath shown in
4 figure 5. However, saturation in the dependence of % EGFP vs. THD is expected because once a
5 cell absorbs the minimum energy needed to express, a further increase in the energy will have no
6 influence in its expression. The maximum % EGFP achieved being lower than 100 % may be
7 related to the inhomogeneous distribution of the MNPs among the cells and in the cell itself. The
8 uptake as measured with VSM is a mean uptake value, actually some cells may be having no
9 MNP incorporated while others may be having large amount of MNPs distributed in many
10 endosomes as it was exemplified in figure 4 for AC-MNPs. Both, the number of filled endosome
11 and their sizes vary within a culture and the compactness of the MNPs inside the endosomes also
12 varies when the MNP is changed. Particularly, less dense endosomes are observed for CA-MNP
13 than for u-MNP. TEM image of A549 cell incubated with u-MNP is shown figure 5 of ESM.

14
15
16
17
18
19
20
21
22
23
24
25
26
27
28
29
30 In general, the total heat released by the MNPs in a cell must be proportional to the amount of
31 MNPs incorporated by the cell, i.e. proportional to the uptake. It must be also proportional to the
32 capacity of these MNPs to absorb energy from the field and release it into the cell, and to the
33 exposure time. Then, the % EGFP appears as an extensive quantity, which is made intensive
34 dividing it by C . On the other hand, at fixed AMF conditions SAR is proportional to $VM_s^2\chi''(\tau)$,
35 i.e. it depends explicitly on the relaxation mechanism through the relaxation time. However, in
36 the case of our particles, the distinctive parameter driving specific heat dissipation is Ms . In
37 figure 8c the plot of %EGFP/ C vs. VM_s^2 displays an increasing behaviour. Recalling that the
38 EGFP expression is due to a thermally-induced stress, as shown in figure 5, the increasing
39 behaviour of %EGFP/ C vs. VM_s^2 suggests that intracellular heat release is occurring, even
40 though the total amount of heat released is not enough to globally increase the temperature of the
41 cell culture. Alternatively, the %EGFP can be plotted vs. $CxMs$, being this quantity the mean

42
43
44
45
46
47
48
49
50
51
52
53
54
55
56
57
58
59
60

1
2
3 magnetic moment of a cell at saturation: $\langle \mu_{\text{sat}} \rangle = N_p V \rho M_s$, where N_p is the mean number of
4
5 particles incorporated per cell. Again, an increasing behaviour is obtained (see figure 8d)
6
7 reinforcing the idea of a direct relationship between the percentage of cells expressing EGFP and
8
9 the intracellular THD and consequently to SAR.
10
11
12
13
14
15
16

17 **Conclusions**

18
19
20 *In vitro* experiments were performed with human lung adenocarcinoma cells (A549 cell line)
21
22 modified with a lentiviral vector that encodes EGFP under the action of the human HSP70B
23
24 promoter. This modified A549 cell line was incubated with three suspensions of magnetite
25
26 nanoparticles displaying distinctive size, saturation magnetization and specific response to
27
28 alternated magnetic fields. Distinctive properties of the same core material were achieved using
29
30 uncoated as well as silicon oxide or citric acid coated nanoparticles. Here we have shown that the
31
32 application of an alternating magnetic field, in the radiofrequency range, to culture cells loaded
33
34 with nanoparticles, resulted in thermal-induced gene expression in the absence of a global
35
36 temperature increase. Stress-inducible gene expression, measured as the amount of cell
37
38 expressing EGFP, increased with the mean magnetic moment of a cell at saturation, with
39
40 nanoparticle volume times the square of saturation magnetization nanoparticle, with thermal heat
41
42 dose and also with nanoparticle heat dissipation ability recorded in the fluid state. All of these
43
44 dependences are linking gene expression to a localized intracellular temperature increase.
45
46
47
48
49
50
51
52
53
54
55
56
57
58
59
60

1
2
3 **Electronic Supplementary Material:** Additional HR-TEM and ED images and the
4
5 corresponding size histograms, SAR frequency dependence and TEM images of A549 cell with
6
7 an endosome loaded with MNPs. This material is available free of charge via the Internet at
8
9 <http://pubs.acs.org/>.
10
11
12
13
14
15
16

17 **Acknowledgements**

18
19
20 This work has been funded by CONICET (PIP 00720), ANPCyT (PICT 00898), UNLP-X11/680
21
22 grants of Argentina.; TEM at Brazilian Nanotechnology National Laboratory (LNNano), Centro
23
24 Nacional de Pesquisa em Energia e Materiais (CNPEM), Brazil under the project TEM-MSC-
25
26 14825. We thank Cátedra de Patología B - CONICET for allowing the use of cell culture lab,
27
28 help in cell culture handling and kind suggestions on biological issues, Roxana Peralta for
29
30 extreme care with cell sample preparation for TEM. P. Mendoza Zélis, F. H. Sánchez, R. A.
31
32 Dewey, R. G. Goya, and M. B. Fernández van Raap are members of CONICET, and M. E. de
33
34 Sousa and A. Carrea are fellows of CONICET, Argentina.
35
36
37
38
39
40
41
42
43

44 **References**

- 45
46
47 [1] Ferlay J, Soerjomataram I, Ervik M, Dikshit R, Eser S, Mathers C, Rebelo M, Parkin DM, Forman D, Bray, F.
48
49 GLOBOCAN 2012 v1.0, Cancer Incidence and Mortality Worldwide: IARC CancerBase No. 11 [Internet].
50
51 Lyon, France: International Agency for Research on Cancer; 2013. Available from: <http://globocan.iarc.fr>, accessed on
52
53 day/month/year.
54
55 [2] Dutz S., Hergt R.. Nanotechnology, Magnetic particle hyperthermia-a promising tumour therapy?. *Nanotechnology*, 2014, 25,
56
57 452001(28pp).
58
59
60

- 1
2
3 [3] Huang X, Jain PK, El-Sayed IH, El-Sayed MA., Plasmonic photothermal therapy (PPTT) using gold nanoparticles. *Lasers*
4 *Med Sci*, **2008**, 23, 217–228.
5
6
7 [4] [Ganta S](#), [Devalapally H](#), [Shahiwala A](#), [Amiji M](#), A review of stimuli-responsive nanocarriers for drug and gene delivery.
8 *Journal of Controlled Release*, **2008**, 126, 187–204.
9
10
11 [5] Sasidharan Swarnalatha Lucky, Khee Chee Soo, and Yong Zhang, Nanoparticles in Photodynamic Therapy. *Chem. Rev.*,
12 **2015**, 115 (4), 1990–2042.
13
14
15 [6] Hilger I., In vivo applications of magnetic nanoparticle hyperthermia. *Int J Hyperthermia*, **2013**, 29(8): 828–834.
16
17
18 [7] Luo S, Wang LF, Ding WJ, Wang H, Zhou JM, Jin HK, Su SF, Ouyang WW. Clinical trials of magnetic induction
19 hyperthermia for treatment of tumours. *OA Cancer*, **2014**, 18;2(1):2.
20
21
22 [8] Villanueva A., de la Presa P., Alonso J. M., Rueda T., Martínez A., Crespo P., Morales M. P., Gonzalez-Fernandez M. A.,
23 Valdés J., Rivero G., Hyperthermia HeLa Cell Treatment with Silica-Coated Manganese Oxide Nanoparticles. *J. Phys. Chem. C*,
24 **2010**, 114, 1976–1981.
25
26
27 [9] I Marcos-Campos, L Asín, T E Torres, C Marquina, A Tres, M R Ibarra, G F Goya. Cell death induced by the application of
28 alternating magnetic fields to nanoparticle-loaded dendritic cells. *Nanotechnology*, **2011**, 22, 205101 (13pp).
29
30
31 [10] Di Corato R., Espinosa A., Lartigue L., Tarahud M., Chat S., Pellegrino T., Menager C., Gazeau F., Wilhelm C.. Magnetic
32 hyperthermia efficiency in the cellular environment for different nanoparticle designs. *Biomaterials*, **2014**, 35, 6400-6411.
33
34
35 [11] Creixell M., Bohorquez A. C., Torres-Lugo M., and Rinaldi C., EGFR-targeted magnetic nanoparticle heaters kill cancer
36 cells without a perceptible temperature rise. *ACS Nano*, **2011**, 5, 7124-7129.
37
38
39 [12] Domenech M., Marrero-Berrios I., Torres-Lugo M., Rinaldi C.. Lysosomal Membrane Permeabilization by Targeted
40 Magnetic Nanoparticles in Alternating Magnetic Fields, *ACS Nano*, **2013**, 7(6) 5091–5101.
41
42
43 [13] Amstad, E.; Kohlbrecher, J.; Muller, E.; Schweizer, T.; Textor, M.; Reimhult, E. Triggered Release from Liposomes through
44 Magnetic Actuation of Iron Oxide Nanoparticle Containing Membranes. *NanoLett*, **2011**, 11, 1664–1670.
45
46
47 [14] Rosensweig R. E., Heating Magnetic Fluid With Alternating Magnetic Field. *J. Magn. Magn. Mater.*, **2002**, 252, 370–374.
48
49
50 [15] Wihelm C., Out-of-Equilibrium Microrheology inside Living Cells, *Phys Rev Lett*, **2008**, 101, 028101(4pp).
51
52
53
54
55
56
57
58
59
60

- 1
2
3 [16] Lau A.W. C., Hoffman B. D., Davies A., Crocker J. C., Lubensky T. C.. Microrheology, Stress Fluctuations, and Active
4 Behavior of Living Cells, *Phys Rev Lett*, **2003**, 91 (19), 198101(4pp).
5
6
7
8 [17] Riedinger A., Guardia P., Curcio A., Garcia M. A., Cingolani R., Manna L., Pellegrino T., Subnanometer Local Temperature
9 Probing and Remotely Controlled Drug Release Based on Azo-Functionalized Iron Oxide Nanoparticles. *Nano Lett.* **2013**, 13,
10 2399-2406.
11
12
13 [18] Donner J. S., Thompson S. A., Kreuzer M. P., Baffou G., and Quidant R., Mapping Intracellular Temperature Using Green
14 Fluorescent Protein. *Nano Lett.* **2012**, 12, 2107–2111
15
16
17
18 [19] de Sousa M. E., Fernández van Raap M. B.; Rivas P. C.; Mendoza Zélis P.; Girardin P., Pasquevich G., Alessandrini J.,
19 Muraca D., Sánchez F. H.. Stability and Relaxation Mechanisms of Citric Acid Coated Magnetite Nanoparticles for Magnetic
20 Hyperthermia. *J. Phys. Chem. C* **2013**, 117 (10), 5436–5445.
21
22
23
24 [20] Mykhaylyk O., Sobisch T., Almstätter I., Sanchez-Antequera Y., Brandt S., Anton M., Döblinger M, Eberbeck D., Settles,
25 Rickmer Braren M, et. al. Silica-Iron Oxide Magnetic Nanoparticles Modified for Gene Delivery: A Search for Optimum and
26 Quantitative Criteria. *Pharm Res*, **2012**, 29(5), 1344-1365.
27
28
29
30 [21] Mykhaylyk O, Sanchez-Antequera Y, Vlaskou D, Hammerschmid E, Anton M, Zelphati O, Plank C. Liposomal
31 magnetofection. *Meth Mol Biol.*, **2010**, 605, 487–525.
32
33
34
35 [22] Noyan F, Avedillo Díez I, Hapke M, Klein C, Dewey R A. Induced transgene expression for the treatment of solid tumors
36 by hematopoietic stem cell-based gene therapy. *Cancer Gene Ther.* **2012**, 5, 352.
37
38
39 [23] Schambach A, Bohne J, Chandra S, Will E, Margison GP, Williams DA, Baum C.. Equal potency of gammaretroviral and
40 lentiviral SIN vectors for expression of O6-methylguanine-DNA methyltransferase in hematopoietic cells. *Mol. Ther*, **2006**, 13,
41 391-400.
42
43
44
45 [24] Wilhelm C., Gazeau F. Universal Cell Labelling With Anionic Magnetic Nanoparticles. *Biomaterials*, **2008**, 29, 3161–3174.
46
47
48 [25] DeNardo, S. J.; DeNardo, G. L.; Natarajan, A.; Miers, L. A.; Foreman, A. R.; Gruettner, C.; Adamson, G. N.; Ivkov, R.
49 Thermal Dosimetry Predictive of Efficacy of ¹¹¹In-ChL6 Nanoparticle AMF-Induced Thermoablative Therapy for Human
50 Breast Cancer in Mice. *J. Nucl. Med.*, **2007**, 48, 437–444.
51
52
53
54
55
56
57
58
59
60

Figures

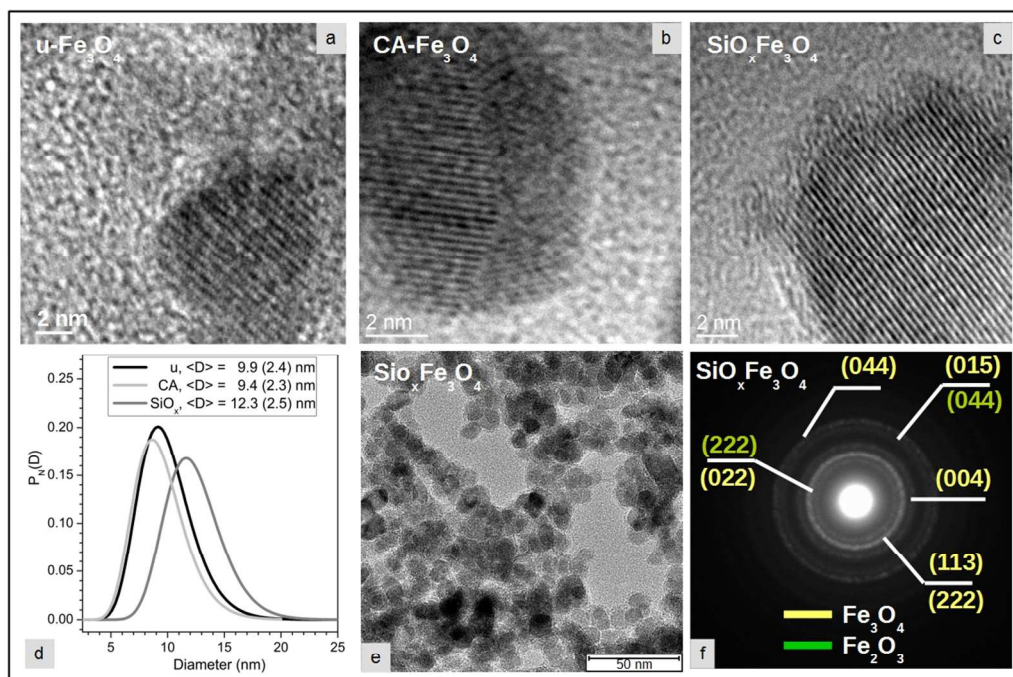


Figure 1: TEM micrographs showing single magnetic particle a) uncoated ($u\text{-Fe}_3\text{O}_4$), b) citric acid-coated ($\text{CA-Fe}_3\text{O}_4$), and c) silicon oxide-coated ($\text{SiO}_x\text{-Fe}_3\text{O}_4$). d) Fitted number size distribution (log-normal) of histograms obtained by measuring more than 120 particles, mean diameter and standard deviation (in parentheses) are indicated. e) Panoramic image for SiO_x -coated MNPs. f) Electron diffraction pattern of SiO_x -coated MNP indexed with the reflection lines of magnetite.

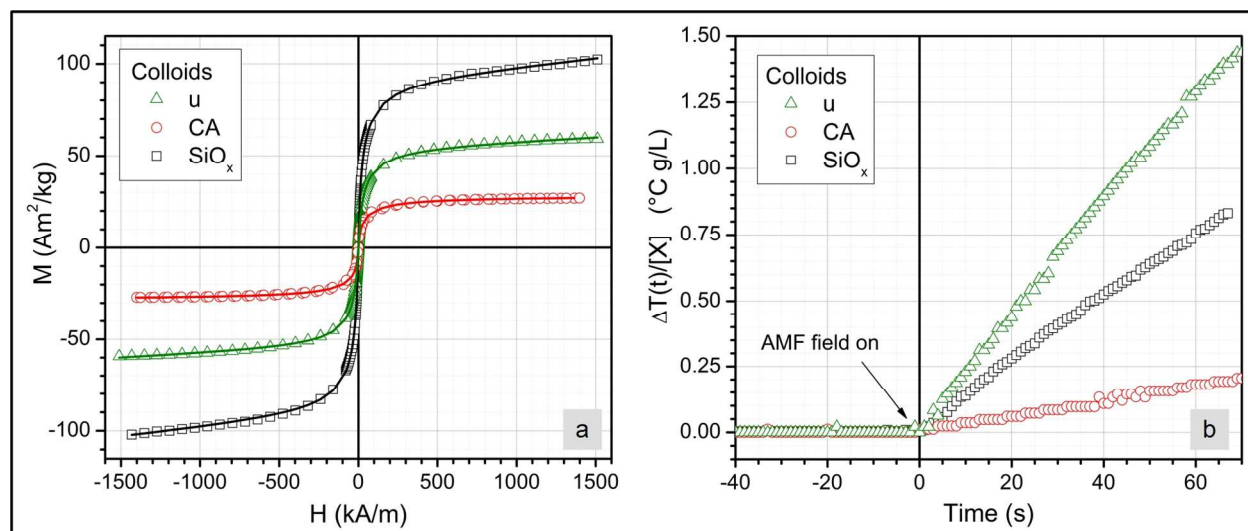
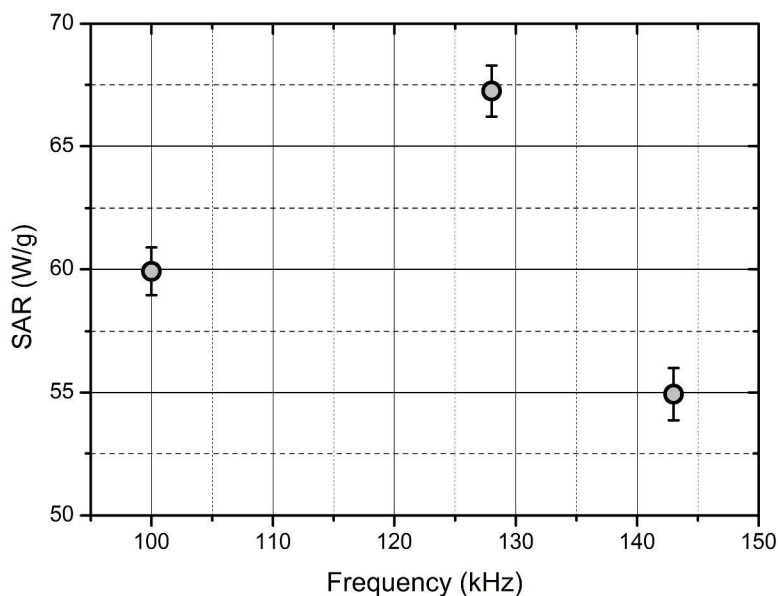
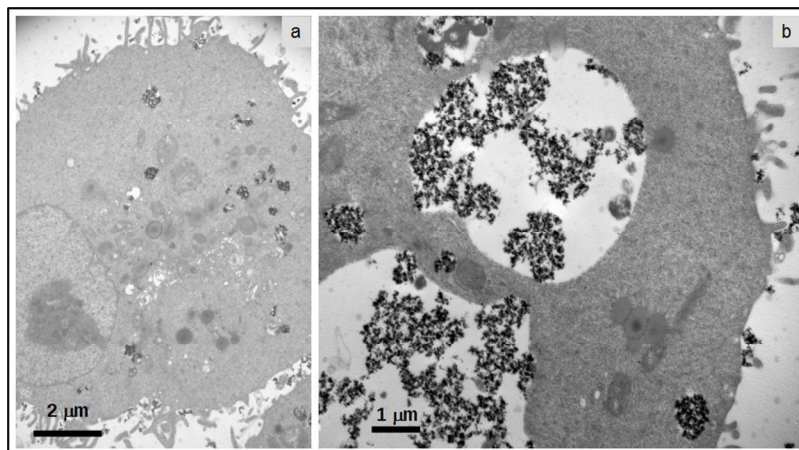


Figure 2: a) Room temperature specific magnetization (M) vs. applied field (H) loops recorded with VMS- dc magnetometry, data was normalized by mass of Fe_3O_4 . b) Heating curves of MNPs aqueous suspensions measured at 128 kHz and 20.3 kA/m. Data is plotted as temperature increase ΔT scaled with concentration $[x]$ vs. time.



1
2
3 **Figure 3:** SAR values in $SiO_x-Fe_3O_4$ aqueous suspensions vs. driven field frequency at a fixed
4
5
6 field amplitude of 20.3 kA/m.
7
8



25
26 **Figure 4:** Nanoparticle-cell interaction characterization. Representative TEM images showing:
27
28 a) the distribution of AC-MNPs inside A549 cell and b) details of MNPs distribution in the cell.
29
30
31
32
33
34
35
36
37
38
39
40
41
42
43
44
45
46
47
48
49
50
51
52
53
54
55
56
57
58
59
60

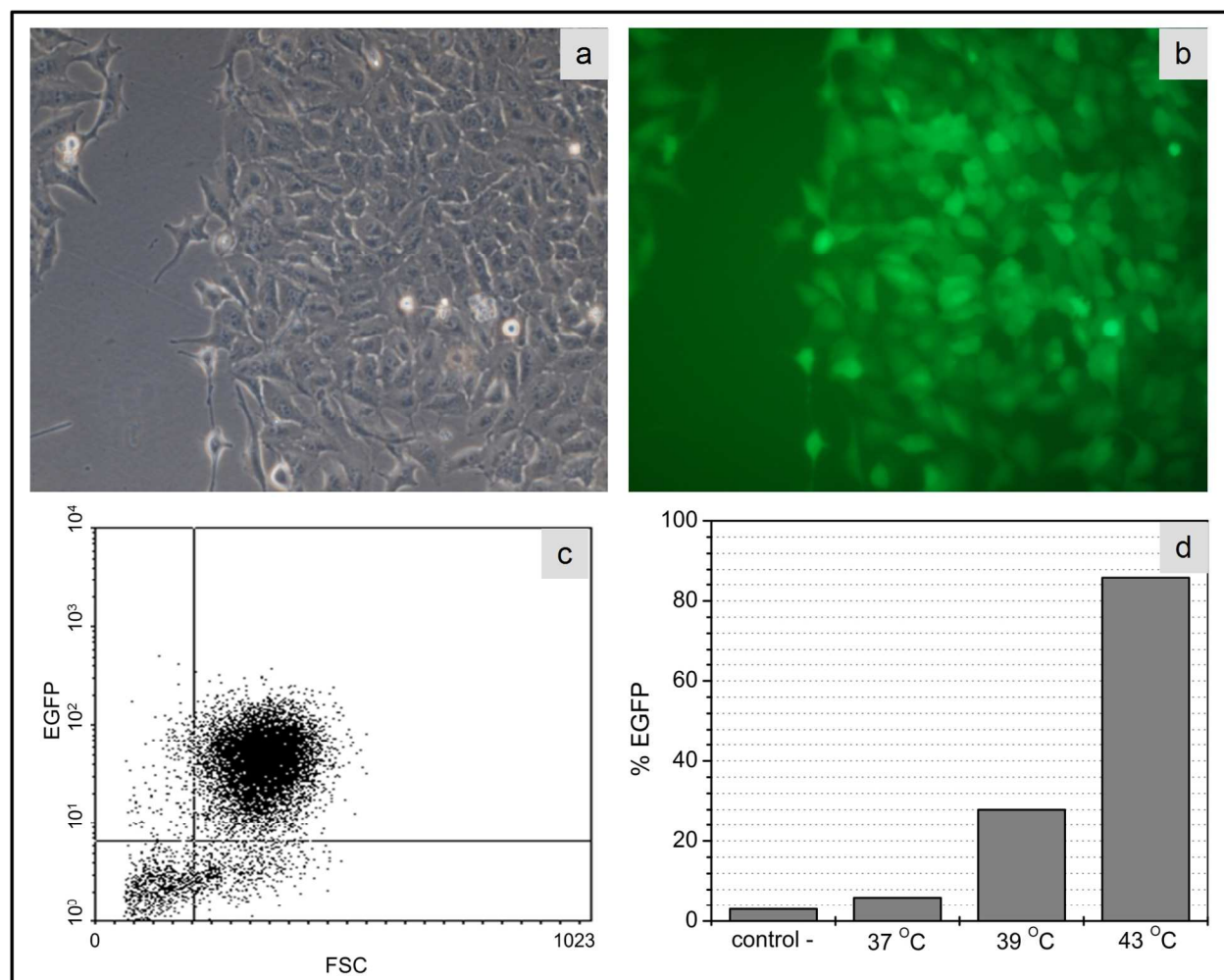


Figure 5: Thermal stress characterization of modified A549^{HSP} cells. a) Phase contrast microscopy image (20X) of A549^{HSP} cells after treatment at 43 °C for 60 min in a thermal bath. b) Fluorescent microscopy image of the A549^{HSP} cells shown in a). c) Flow cytometry dot-plot showing EGFP expression vs. forward scattered (FSC). d) %EGFP is the percentage (relative to the total analyzed cells) of cells expressing EGFP, in A549^{HSP} cultures treated at 37, 39 and 43 °C for 60 min. Control - stands for negative control, i.e. untreated cells.

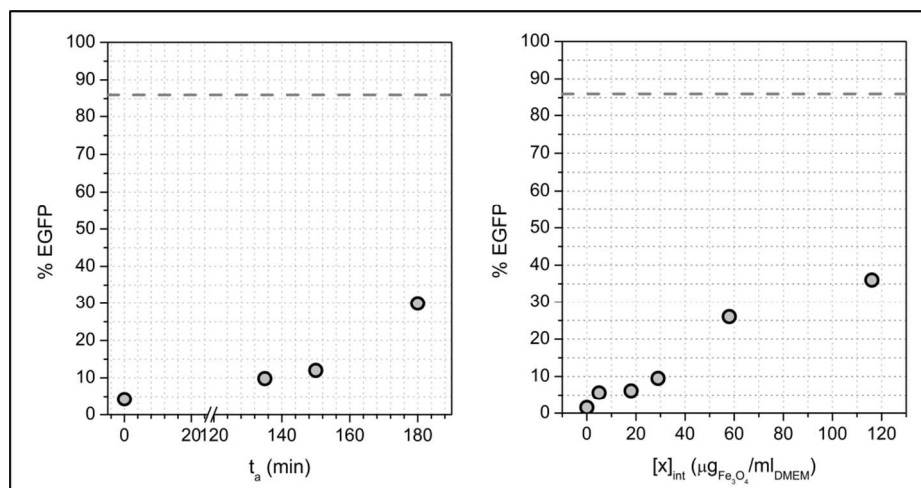


Figure 6: Characterization of alternating magnetic field and nanoparticles gene stress induction.

Percentage of cells expressing EGFP (%EGFP) a) after exposure of unloaded A549^{HSP} cells to an AMF of 128 kHz and 20.3 kA/m for time intervals t_a , and b) after incubation of A549^{HSP} cells in medium doped with $SiO_x-Fe_3O_4$ colloidal suspension of concentration $[x]_{int}$. For comparison, the value of thermal treatment at 43 °C for 1 h is included (dotted lines).

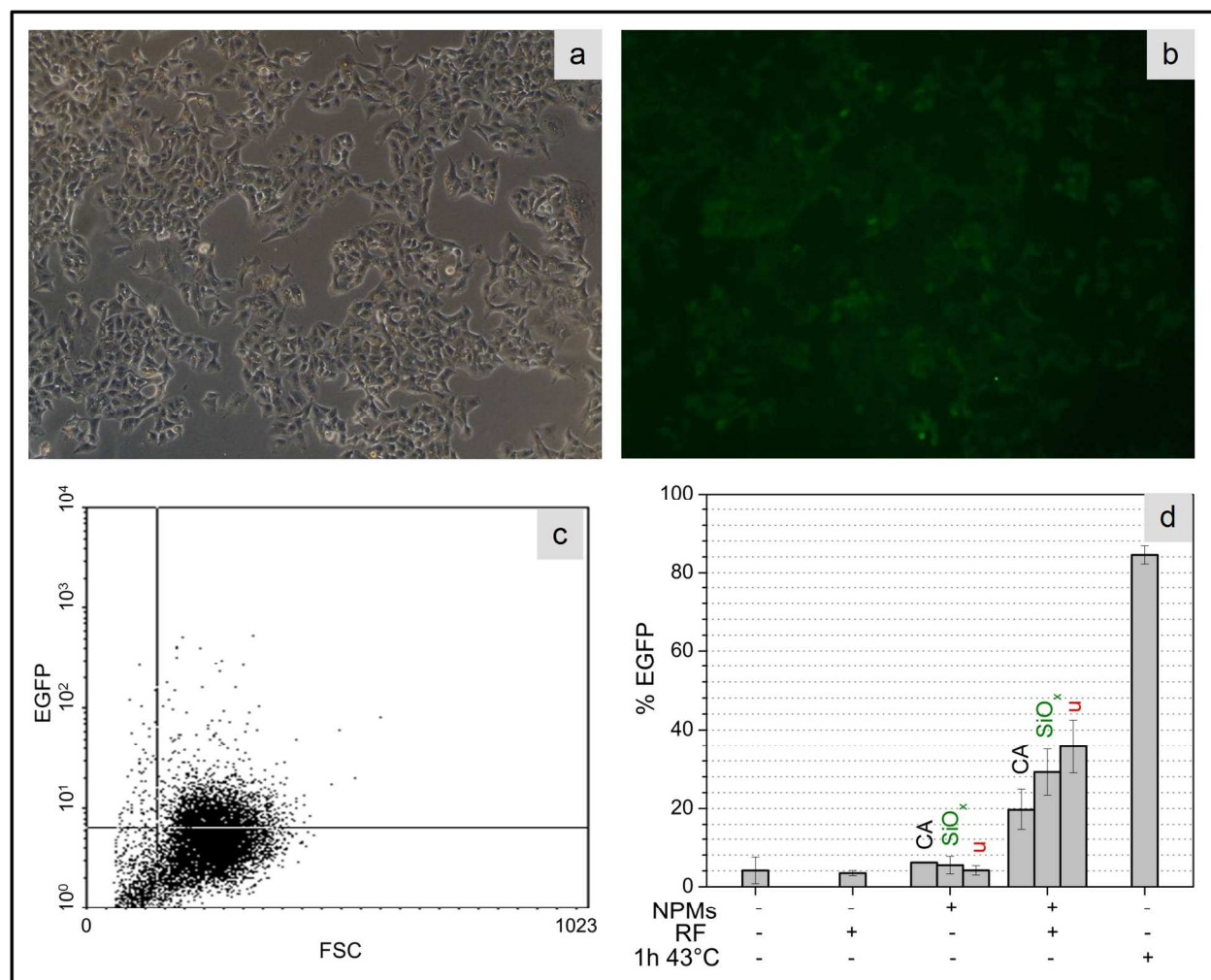


Figure 7: a) Phase contrast microscopy image (20X) of A549^{HSP} cells after incubation with MNPs and AMF treatment. b) Fluorescent microscopy image of the A549^{HSP} cells shown in a). c) Flow cytometry dotplot showing EGFP expressing cells vs. forward scattered (FSC). d) Bar graph displaying the percentages of cells expressing EGFP (%EGFP) in A549^{HSP} cell culture, from left to right, incubated without MNPs and not exposed to any AMF or to thermal treatment (negative control), cells exposed to an AMF of 128 kHz and 20.3 kA/m (AMF-control) for 135 min, cells incubated for 17 h in medium doped with MNPs at a concentration of 29 $\mu\text{g}_{\text{Fe}_3\text{O}_4}/\text{ml}_{\text{DMEM}}$ (MNPs-control), cells incubated with MNPs at a concentration of 29 $\mu\text{g}_{\text{Fe}_3\text{O}_4}/\text{ml}_{\text{DMEM}}$ and exposed to an AMF of 128 kHz and 20.3 kA/m for 135 min (HM-experiment), and cell treated in 29

thermal bath at 43 °C for 60 min (positive control). Data is shown as mean \pm SD of two independent experiments, and statistically analyzed using Student's *t* test.

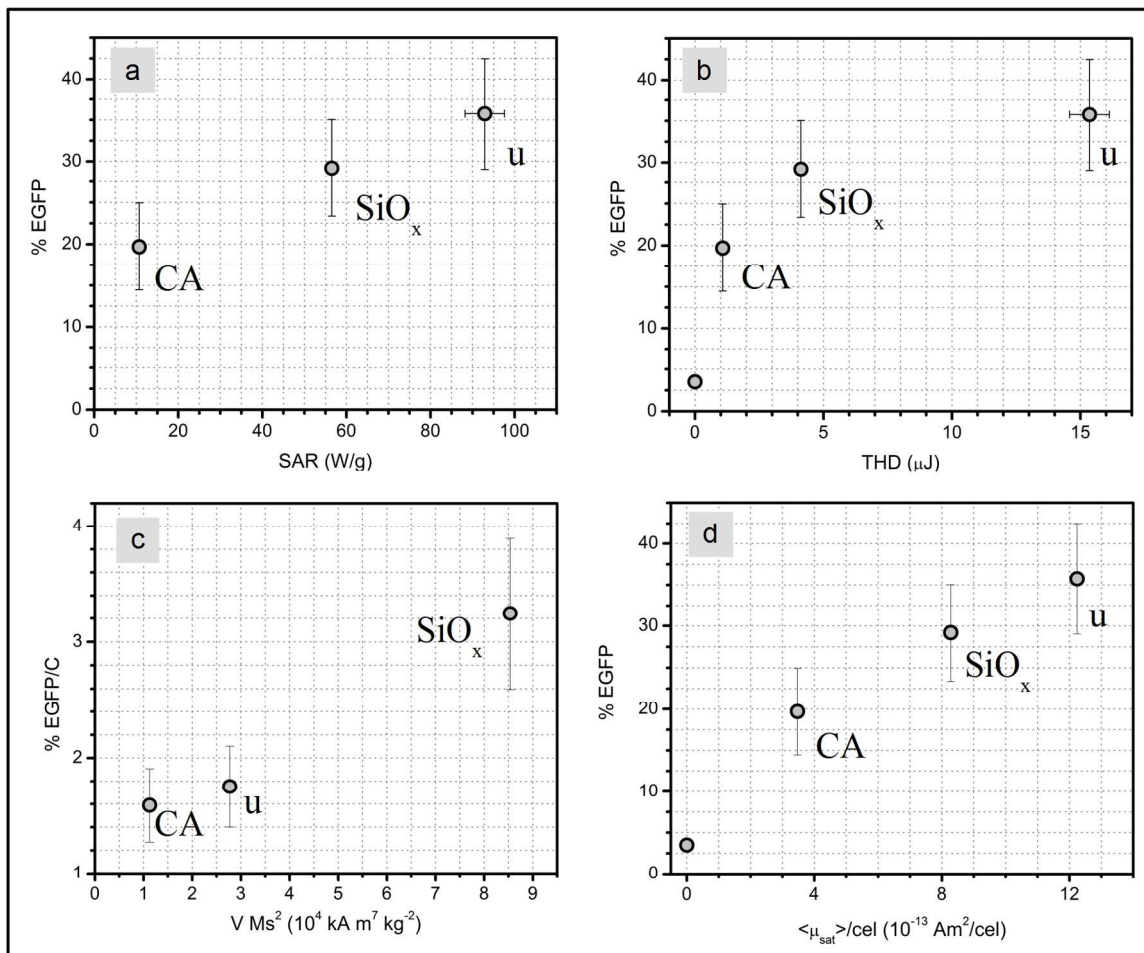


Figure 8: Percentage of cells expressing EGFP (%EGFP) vs. a) SAR; b) total heat dose (THD) per cell, i.e. MNP energy released per cell due to exposure to an AMF (data from control AMF culture is included with null assigned energy). c) Specific variable %EGFP/C defined as % EGFP divided by the uptake C vs. the square of nanoparticle saturation magnetization (M_s) times the MNP volume (V). d) Percentage of cells expressing EGFP (% EGFP) vs. the mean magnetic moment of a cell at saturation, $\langle \mu_{\text{sat}} \rangle$.

Tables

MNP	[x] (mg _{MNP} /ml)	<D> nm	Ms (Am ² /kg)	SAR (W/g _{MNP})
CA-Fe ₃ O ₄	8.3	9.4	28	10.7(0.6)
u-Fe ₃ O ₄	4.8	9.9	60	92.9(4.5)
SiO _x -Fe ₃ O ₄	22.5	12.3	92	67.3(1.0)

Table 1: Colloid and nanoparticle properties. MNP: type of magnetic nanoparticle, [x] is the concentration expressed in mg of Fe₃O₄ per mL of water, <D> is the mean MNP size determined from HRTEM histograms shown in the ESM, Ms: saturation magnetization expressed per mass of Fe₃O₄, and SAR: specific absorption rate measured in the colloidal suspensions at 128 kHz and 20.3 kA/m.

MNP	C (pg/cell)	EGFP (%)	EGFP/C (cell/pg)	CxMs=<μ _{sat} >/cell (10 ⁻¹⁵ Am ² /cell)	THD (μJ/cell)
CA- Fe ₃ O ₄	12.4(2.5)	20(5)	1.6(0.5)	347	1.16(0.06)
u-Fe ₃ O ₄	20.4(4.1)	36(7)	1.8(0.4)	1224	15.32(0.08)
SiO _x Fe ₃ O ₄	9.0(1.8)	29(6)	3.2(0.9)	828	4.08(0.08)

Table 2: Nanoparticle-cell interaction and interrelation between EGFP and the physical characterization. C is the A549^{HSP} uptake after 17 h incubation in 29 μg/ml_{DMEM} of Fe₃O₄, SiO_x-Fe₃O₄ or AC-Fe₃O₄. Percentage of A549^{HSP} cells expressing EGFP after incubation with MNPs and AMF treatment (f=128 kHz, H₀=20.3 kA/m). THD is the total heat dose per cell, i.e. the energy released by the MNP per cell due to exposure to the AMF.

Graphical Table of Contents